

Low- Q^2 nucleon structure from an infrared-safe evolution scheme

Rong Wang^{1, 2, *}

¹*Institute of Modern Physics, Chinese Academy of Sciences, Lanzhou 730000, China*

²*School of Nuclear Science and Technology, University of Chinese Academy of Sciences, Beijing 100049, China*

(Dated: October 2, 2024)

The low- Q^2 nucleon structure is given with a simple nonperturbative input of three valence quarks and an all-order infrared-safe evolution scheme, showing some consistencies with the experimental data. The resonance peaks in the experimental data of F_2 structure function are found to be modulated by the valence quark distributions. With little sea quark distribution at low Q^2 the valence-quark bump is clearly shown in the structure function. The three valence quark distributions at the hadronic scale is found to be the dominant origin of the PDFs at the hard scales. The high-twist corrections are needed to explain the sizeable discrepancy between the theory and the experimental measurements at low Q^2 . The infrared-safe evolution scheme is a powerful tool for connecting the nucleon structures in the nonperturbative and perturbative regions.

I. INTRODUCTION

Mapping the nucleon structure precisely is a hot topic in particle and nuclear physics, as it is closely related to the intricate and puzzling nonperturbative phenomena, such as the emergent hadron mass [1–6] and the color confinement [7–11]. With the advent of Electron-Ion Collider (EIC) in the near future [12, 13], the proposed Electron-ion collider in China (EicC) [14–17] and JLab 24 GeV upgrade [18], the nucleon structure will be measured much more precisely in a broad kinematic region with multi-dimensional information, to finally tackle the challenging issues on the strong interaction in the non-perturbative region. The study of nucleon structure is essential for full understanding of the complex dynamics of the strong interaction, of which the underlying theory is quantum chromodynamics (QCD) [19–23].

The core base for describing the nucleon structure is parton distribution function (PDF) $f(x)$ [24–27], defined as the number density of the partons carrying x fraction of the longitudinal momentum of the nucleon in the infinite-momentum frame (or light-cone momentum). Actually, the precision determinations of PDFs from global analyses [28–31] have been a remarkable milestone of QCD theory. Yet, the origin of PDFs and the evolution of nucleon structure in the infrared region are not fully resolved. The nucleon structure can be easily and economically evaluated at low Q^2 , for the degrees of freedom of sea quark and gluon fluctuations are frozen. However, how to link the calculations in the infrared region to the experimental measurements at high scales lacks comprehensive studies.

There is no doubt that the nonperturbative effects should be implemented for the PDF evolution with the Q^2 scale in low- Q^2 domain. Recently, an infrared-safe evolution scheme is proposed to soundly extend the QCD evolution to $Q^2 \approx 0$ GeV 2 [32], with the effects of effective parton mass, saturating running strong coupling,

and parton-parton recombination. This kind of evolution is also argued to be all-order exact [33]. Under this novel evolution scheme, the PDFs are delivered consistently in the whole Q^2 range from 0 GeV 2 to infinity. With the help of the new evolution scheme, firstly, we would like to check the origin of PDFs. According to the quark model assumption, the nucleon is made of three quarks, which are the minimum number of quarks forming a color singlet. Without the contributions of sea quark and gluon distributions, the bump of valence quark distribution should show up in the structure function at extremely low Q^2 . Secondly, for example, the valence quark distributions estimated in infrared region from maximum entropy method [34] are tested using the suggested infrared-safe evolution equations. The third aim of this study is to check the violation of factorization [35–37], via the comparisons between the theoretical predictions and the experimental measurements of structure function F_2 at the low Q^2 scales.

The organization of the paper is as follows. The input valence quark distributions at the hadronic scale and the nonperturbative effects within the Continuum Schwinger Methods (CSMs) [6] are discussed in Sec. II. How the nonperturbative effects modify the evolution equations and the elicited infrared-safe evolution equations are demonstrated in Sec. III. The predicted F_2 structure functions at low Q^2 are shown and compared with JLab data [38] in Sec. IV. The discussions on the origin of PDFs and the factorization invalidity at low Q^2 are also provided in Sec. IV. A concise summary is provided in Sec. V.

II. NONPERTURBATIVE EFFECTS

All the complex strong interaction dynamics at long distance are reflected in the nonperturbative input of PDFs. The nonperturbative input is the initial PDFs at the hadronic scale, and the hadronic scale is defined as the scale where the nucleon contains only the valence and minimal components. The nonperturbative input is related to the nucleon wave function at the low energy

* rwang@impcas.ac.cn

scale governed by the nonperturbative strong interaction.

Dynamical chiral Symmetry Breaking (DCSB) is a prominent phenomenon in QCD [4, 39–46], which offers a mechanism of generating mass from nothing. In the chiral limit, a quark acquires the massive mass through the strong interactions with gluons at the low momentum scale. By evaluating the two-point Green function of quark, both CSMs and LQCD give the excellent and mutual consistence regarding the features of DCSB [44]. The large effective mass of quark definitely affects the splitting kernels of the evolution equations that are derived under the assumption of massless quarks. DCSB is one unavoidable nonperturbative effect in the infrared region.

To perform the calculations in the infrared region, an infrared finite strong coupling is needed. According to the recent definition of QCD effective charge [47, 48], the running strong coupling saturates up to a finite value in the infrared region, for the Landau pole is tamed due to the massive effective mass of gluon at low momentum. The saturating α_s is one important ingredient of our calculations.

A. Nonperturbative input of PDFs

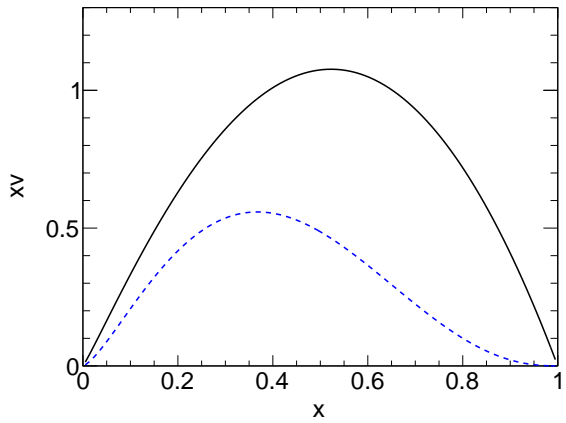


FIG. 1. The input parton distributions of mere valence quarks at the sufficiently low Q_0^2 scale. The solid and dashed curves show the up and down valence quark distributions respectively.

It is very convenient to compute the nucleon structure at an extremely low Q^2 scale by reason of the minimal constituents inside the nucleon at the scale. Nowadays, the nonperturbative input can be estimated with the first principle techniques of CSMs [49–53] and Lattice QCD simulation [54–59], and many other model calculations [34, 60–66]. For the simplicity of calculation, the nonperturbative input from the maximum entropy method (MEM) [34] is used in this work. Actually, there is no

much difference by using different nonperturbative inputs.

Fig. 1 shows the simplest nonperturbative input of just three valence quarks at extremely low Q^2 scale, where only the valence components in the nucleon can be resolved or probed. The input three valence quark distributions is evaluated with MEM, under the constraints of the quark model assumption and the confinement radius of quarks [34]. This MEM nonperturbative input is found to be more or less consistent with the global fits and the experimental data [34].

B. Dressed parton mass

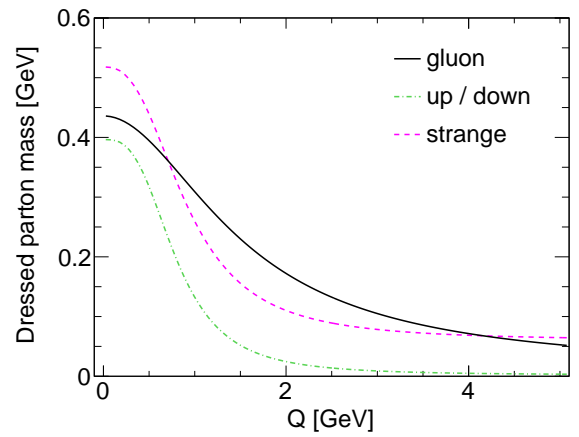


FIG. 2. The dressed parton mass as a function of the momentum [4, 67]. The types of the partons are indicated in the figure.

The effective masses of quark and gluon are important parameters for the modifications of splitting kernels of QCD evolution equations in the infrared region. For DCSB, the quark mass is a smooth function of the momentum. The mass functions of quark and gluon can be evaluated with Dyson-Schwinger equations which take into account the contributions of infinite diagrams [4, 67]. Usually, the symmetry-preserving truncation of the diagrams (Rainbow-Ladder truncation) is applied in the calculations [46, 68]. Nevertheless, Dyson-Schwinger equations predict the quark mass function that is amazingly consistent with LQCD simulations.

Fig. 2 shows the dressed quark and gluon mass functions from CSMs [4, 67]. One sees that the dressed quark mass decreases monotonically with the increasing momentum. The constituent quark mass is smoothly connected with the current quark mass under the DCSB mechanism of complex strong interaction dynamics. In this work, the parametrization forms of these mass functions are used in the following calculations of the infrared-safe evolution equations.

C. Saturating running strong coupling

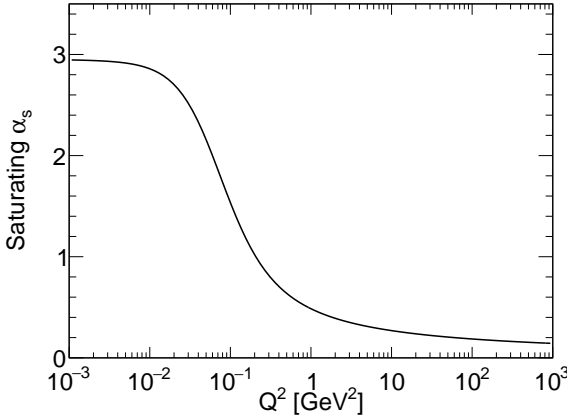


FIG. 3. The saturating running strong coupling α_s as a function of the Q^2 scale [4, 47, 48, 53]. The running coupling saturates in the far-infrared region around π .

The running strong coupling α_s is a key parameter for any QCD processes. To get rid of the divergent problem of perturbative α_s , we capitalize a renormalization-group-invariant and process-independent effective charge in QCD [4, 47, 48, 53]. Based on the concept of QCD effective charge, the infrared behavior of α_s is quite different from the traditional perturbative α_s . The QCD effective charge derives a saturating α_s which is free of Landau pole. The screening effect is suppressed at long distance due to the big effective mass of the gluon. In this work, the saturating α_s is applied in the calculations of infrared-safe evolution equations.

Fig. 3 shows the saturating α_s from CSMs [4, 47, 48, 53]. This saturating α_s provides an infrared completion with $\alpha_s/\pi \sim 0.97$ in the infrared limit. At high Q^2 , the saturating α_s agrees well with the perturbative α_s . According to the recent calculations of CSMs, a parametrization of saturating α_s is given by [4, 47, 48, 53],

$$\begin{aligned} \alpha_s &= \frac{\gamma_m \pi}{\ln[\mathcal{K}^2(k^2)/\Lambda_{\text{QCD}}^2]}, \\ \mathcal{K}(y) &= \frac{a_0^2 + a_1 y + y^2}{b_0 + y}, \end{aligned} \quad (1)$$

where the parameters are $\gamma_m = 4/\beta_0$, $\beta_0 = 11 - (2/3)n_f$, and $\Lambda_{\text{QCD}} = 0.234$ GeV.

III. AN INFRARED-SAFE EVOLUTION SCHEME

Considering the nonperturbative effects discussed above, we have proposed a novel and infrared-safe evolution scheme [32]. The massive parton mass hinders

the parton radiation processes in Dokshitzer-Gribov-Lipatov-Altarelli-Parisi (DGLAP) evolution [69–71] over the Q^2 scale. The evolution speed is controlled with a factor $Q^2/(Q^2 + M_q^2)$, where M_q is the quark effective mass provided by DCSB. The saturating α_s offers us a finite interaction strength in QCD at any given momentum scale. The last ingredient for the infrared-safe evolution scheme is the parton-parton recombination correction [72–74]. The parton-parton recombination process balances the parton splitting process, slowing down the growth of gluon distribution at small x , ensuring the cross section unitarity restored at high energy. Due to the large parton size at low Q^2 , the parton-parton overlapping effect should not be ignored at the low scales.

With the implementations of the nonperturbative effects and the parton-parton overlapping effect, we finally get an infrared-safe evolution scheme which works at any given Q^2 scale. In this work, the infrared-safe evolution scheme is applied to a MEM nonperturbative input, so as to deliver the nucleon PDFs at the low Q^2 scales. The infrared-safe evolution equations are written as,

$$\frac{dxq_i^{\text{NS}}}{d\ln(Q^2)} = \frac{Q^2}{Q^2 + M_q^2} \frac{\alpha_s(Q^2)}{2\pi} P_{qq} \otimes xq_i^{\text{NS}}, \quad (2)$$

for the flavor non-singlet quark distributions,

$$\begin{aligned} \frac{dx\bar{q}_i}{d\ln(Q^2)} &= \frac{Q^2}{Q^2 + M_q^2} \frac{\alpha_s(Q^2)}{2\pi} [P_{qq} \otimes x\bar{q}_i + P_{qg} \otimes xg] \\ &- \frac{Q^2}{Q^2 + M_q^2} \frac{\alpha_s^2(Q^2)}{4\pi R^2 Q^2} \int_x^{1/2} \frac{dy}{y} xP_{gg \rightarrow \bar{q}}(x, y)[yg(y, Q^2)]^2 \\ &+ \frac{Q^2}{Q^2 + M_q^2} \frac{\alpha_s^2(Q^2)}{4\pi R^2 Q^2} \int_{x/2}^x \frac{dy}{y} xP_{gg \rightarrow \bar{q}}(x, y)[yg(y, Q^2)]^2, \end{aligned} \quad (3)$$

for the sea quark distributions, and

$$\begin{aligned} \frac{dxg}{d\ln(Q^2)} &= \frac{Q^2}{Q^2 + M_g^2} \frac{\alpha_s(Q^2)}{2\pi} [P_{gq} \otimes x\Sigma + P_{gg} \otimes xg] \\ &- \frac{Q^2}{Q^2 + M_g^2} \frac{\alpha_s^2(Q^2)}{4\pi R^2 Q^2} \int_x^{1/2} \frac{dy}{y} xP_{gg \rightarrow g}(x, y)[yg(y, Q^2)]^2 \\ &+ \frac{Q^2}{Q^2 + M_g^2} \frac{\alpha_s^2(Q^2)}{4\pi R^2 Q^2} \int_{x/2}^x \frac{dy}{y} xP_{gg \rightarrow g}(x, y)[yg(y, Q^2)]^2, \end{aligned} \quad (4)$$

for the gluon distribution, where P_{qq} , P_{qg} , P_{gg} , P_{gq} are the standard splitting kernels, and $P_{gg \rightarrow \bar{q}}$, $P_{gg \rightarrow g}$ are the gluon-gluon recombination kernels. The factor $1/(4\pi R^2)$ in the equations is for two-parton density normalization, and R is the correlation length of two overlapping partons fixed already in a previous study [31].

In above equations, the factor $Q^2/(Q^2 + M_{q/g}^2)$ quenches the evolution at low Q^2 , where $M_{q/g}(Q^2)$ denote the mass functions offered from CSMs. The factor $Q^2/(Q^2 + M_{q/g}^2)$ comes from the modifications of the standard evolution kernels (the splitting and recombination processes). As $Q^2/(Q^2 + M_{q/g}^2)$ is not x -dependent,

we take it out from the integrals on the right sides of the equations. The $\alpha_s(Q^2)$ is the saturating α_s given in Eq. (1). It is finite at any Q^2 scale. The terms with $\int_x^{1/2}$ come from the gluon-gluon recombination processes which reduce the growth of parton density. The terms with $\int_{x/2}^x$ are the anti-shadowing contributions to keep the momentum conservation in the gluon-gluon recombination processes.

IV. RESULTS AND DISCUSSIONS

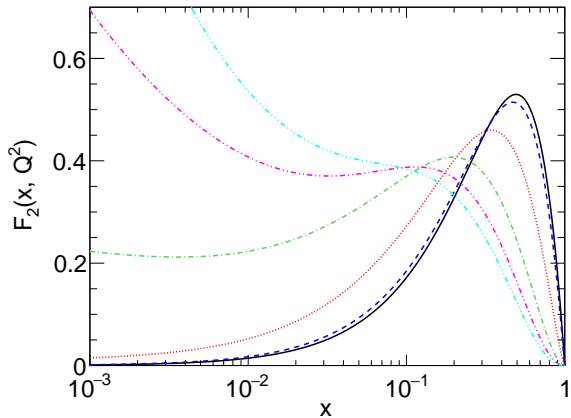


FIG. 4. The obtained F_2 structure function as a function of x at different scales from the infrared-safe evolution equation. The Q^2 scales are at 0.001 (solid), 0.01 (dashed), 0.1 (dotted), 1 (dashed-dotted), 10 (dashed-dotted-dotted), 100 GeV^2 (dashed-dotted-dotted-dotted), respectively.

One prominent feature of the infrared-safe evolution scheme is the freeze of PDF evolution as Q^2 approaching zero, explicitly indicated with the factor $Q^2/(Q^2 + M_{q/g}^2)$. It is found that the evolved PDFs are not sensitive to the choice of input hadronic scale Q_0^2 , so long as $Q_0^2 \lesssim 0.1 \text{ GeV}^2$. Owing to the freeze of PDF evolution in the region of $Q^2 \approx 0 \text{ GeV}^2$, a naive and natural choice of the hadronic scale is $Q_0^2 = 0 \text{ GeV}^2$. In the following calculations, we set $Q_0^2 = 0.0001 \text{ GeV}^2$ for a fast calculation of PDFs to a high Q^2 scale.

The infrared-safe evolution equation is applied to the three valence quark distributions from MEM at $Q_0^2 = 0.0001 \text{ GeV}^2$, to obtain the PDFs at higher Q^2 . With the evolved PDFs, the proton structure functions are then computed at different Q^2 scales, which are shown in Fig. 4. One sees that the structure function peaks in the valence region at low Q^2 scales, due to the tiny sea quark distribution at low scale. Thus, the valence-quark bump in F_2 structure function at low Q^2 is a strong proof of that the dominant valence quark distributions are the origin of the PDFs measured at the hard scales. In other words, the quark model description of the nucleon is the origin of the asymptotic partons in the infinite momentum frame.

Our predicted structure functions are compared to JLab measurement [38] at the low Q^2 scales in the large x region, which is shown in Fig. 5. At finite Q^2 , the target mass effect modifies the identification of the Bjorken variable x with the light-cone momentum fraction. It was argued that the effect of the finite target mass can be removed by analyzing the structure functions in terms of the Nachtmann variable [75, 76], which is defined as $\xi = 2x/[1 + \sqrt{1 + 4x^2 M_N^2/Q^2}]$, where M_N is the nucleon mass. One sees that at high Q^2 , ξ and x are almost identical. Therefore, we show the measured structure function at low Q^2 as a function of ξ . In Fig. 5, one finds that the experimental data is obviously lower than the theoretical predictions. However, the resonance peaks in the experimental data are amazingly well modulated with our theoretical predictions. This indicates that the quark-hadron duality exists at low Q^2 and our theoretical calculations are consistent with the experimental data approximately.

Judged from the JLab data at different Q^2 [38], one sees clearly the valence-quark bump in the measured structure function, regardless the fluctuations caused by the resonances. The heights of the resonance peaks are well described with the overwhelming valence quark distribution in the low- Q^2 region. According to quark-hadron duality, the experimental data at low Q^2 can be interpreted roughly with the three valence quark distributions. To conclude, the quark model description in the infrared region is the dominant origin for the asymptotic partons observed at high energies.

In fact, we could modify the input three valence quark distributions to explain the low- Q^2 data slightly better. Nonetheless, the inherent inconsistency can not be removed by just tuning the nonperturbative input at Q_0^2 . Moreover, the lower the Q^2 is, the larger the discrepancy between the theory and the data is found. The theoretical calculations are provided under the factorization theorem. Thereby, from this study, we conclude that the lower the Q^2 is, the more significant violation of the factorization theorem is found. Of course, this finding is not surprising, since at low Q^2 the sizeable high-twist correction is not included in the factorization formula. To improve the interpretations of the low- Q^2 data, the study of high-twist contributions is quite necessary.

V. SUMMARY

An infrared-safe evolution scheme is applied to the initial three valence quark distributions at Q_0^2 , to study the origin of PDFs. The three valence quarks in the quark model is found to be the dominant origin of the exquisite PDFs at the hard scales. Regardless of the structures of resonances in the data, the JLab experiment has shown a clear valence-distribution bump in the measured F_2 structure function at low Q^2 scales. The quark-hadron duality is observed as well.

The infrared-safe evolution scheme is an essential

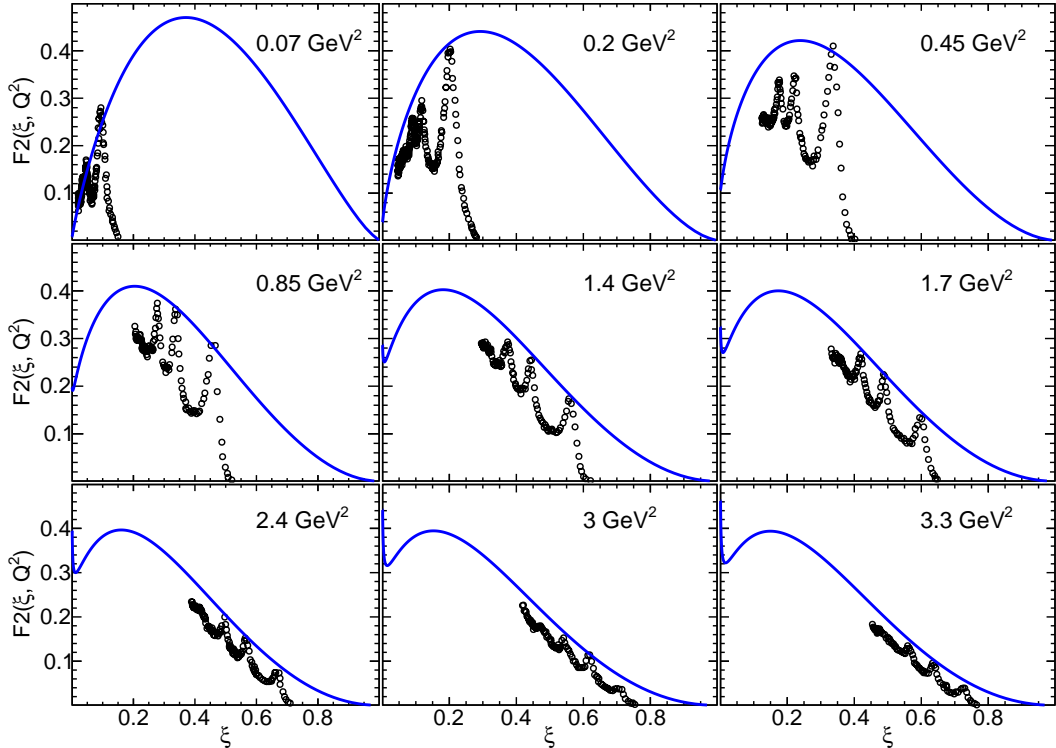


FIG. 5. The F_2 structure function as a function of Nachtmann variable ξ at low Q^2 scales in the large x region. The circles show the experimental data from JLab [38]. The curves show the predictions from the infrared-safe evolution scheme.

bridge for connecting the nucleon structures in the non-perturbative region and perturbative region. The massive dressed quark mass, the saturating α_s , and the parton-parton overlapping corrections are important for the validity and success of the infrared-safe evolution scheme. Via the infrared-safe evolution scheme, the quark model is smoothly linked to the parton model, and the nucleon PDFs can be delivered in the whole momentum range from 0 GeV^2 to any given high scales.

In this study, the factorization violation at low Q^2 is observed and tested with the JLab experimental data. Consistent with the suppression behavior of high-twist contributions, the higher the Q^2 is, the smaller the violation is seen. The quantitative study of the high-twist phenomenon is looking forward to improve the theoretical explanation of the low- Q^2 data. Although the factorization is violated at low Q^2 , the PDFs still exist at

low Q^2 guaranteed by the definition of the matrix elements of bilocal light-cone operators. By extracting the leading-twist contribution to the structure function from the PDFs, we could get some valuable information on the high-twist corrections at low Q^2 scales.

The low- Q^2 nucleon structure given in this work and the high-twist QCD corrections can be further studied and tested on the future high-energy facilities, such as EIC [12, 13], EicC [14–17], and JLab 24 GeV program [18]. In order to access the small Q^2 data, the electrons of very small angles should be measured efficiently. Judged by the difficulty of detecting the small-angle electrons, the low-energy EicC is a little more appropriate to access the low- Q^2 data on the nucleon structure. More high-precision experiential data are looking forward to finally solve the problems regarding the transition from the nonperturbative region to the perturbative region.

-
- [1] M. Ding, C. D. Roberts, and S. M. Schmidt, Particles **6**, 57 (2023), arXiv:2211.07763 [hep-ph].
[2] J. Papavassiliou, Chin. Phys. C **46**, 112001 (2022), arXiv:2207.04977 [hep-ph].
[3] D. Binosi, Few Body Syst. **63**, 42 (2022), arXiv:2203.00942 [hep-ph].
[4] C. D. Roberts, D. G. Richards, T. Horn, and L. Chang, Prog. Part. Nucl. Phys. **120**, 103883 (2021), arXiv:2102.01765 [hep-ph].
[5] D. S. Carman, R. W. Gothe, V. I. Mokeev, and C. D. Roberts, Particles **6**, 416 (2023), arXiv:2301.07777 [hep-ph].
[6] C. D. Roberts and A. G. Williams, Prog. Part. Nucl. Phys. **33**, 477 (1994), arXiv:hep-ph/9403224.

- [7] K. G. Wilson, Phys. Rev. D **10**, 2445 (1974).
- [8] M. Bander, Phys. Rept. **75**, 205 (1981).
- [9] G. 't Hooft, Nucl. Phys. B **190**, 455 (1981).
- [10] A. M. Polyakov, Nucl. Phys. B **120**, 429 (1977).
- [11] S. Mandelstam, Phys. Rept. **23**, 245 (1976).
- [12] R. Abdul Khalek et al., Nucl. Phys. A **1026**, 122447 (2022), arXiv:2103.05419 [physics.ins-det].
- [13] A. Accardi et al., Eur. Phys. J. A **52**, 268 (2016), arXiv:1212.1701 [nucl-ex].
- [14] X. Chen, PoS **DIS2018**, 170 (2018), arXiv:1809.00448 [nucl-ex].
- [15] X. Chen, F.-K. Guo, C. D. Roberts, and R. Wang, Few Body Syst. **61**, 43 (2020), arXiv:2008.00102 [hep-ph].
- [16] D. P. Anderle et al., Front. Phys. (Beijing) **16**, 64701 (2021), arXiv:2102.09222 [nucl-ex].
- [17] R. Wang and X. Chen, Few Body Syst. **63**, 48 (2022).
- [18] A. Accardi et al., Eur. Phys. J. A **60**, 173 (2024), arXiv:2306.09360 [nucl-ex].
- [19] D. J. Gross and F. Wilczek, Phys. Rev. Lett. **30**, 1343 (1973).
- [20] H. D. Politzer, Phys. Rev. Lett. **30**, 1346 (1973).
- [21] C.-N. Yang and R. L. Mills, Phys. Rev. **96**, 191 (1954).
- [22] H. Fritzsch, M. Gell-Mann, and H. Leutwyler, Phys. Lett. B **47**, 365 (1973).
- [23] G. 't Hooft and M. J. G. Veltman, Nucl. Phys. B **44**, 189 (1972).
- [24] R. L. Workman et al. (Particle Data Group), PTEP **2022**, 083C01 (2022).
- [25] J. D. Bjorken, Phys. Rev. **179**, 1547 (1969).
- [26] R. P. Feynman, Phys. Rev. Lett. **23**, 1415 (1969).
- [27] J. D. Bjorken and E. A. Paschos, Phys. Rev. **185**, 1975 (1969).
- [28] R. D. Ball, V. Bertone, F. Cerutti, L. Del Debbio, S. Forte, A. Guffanti, J. I. Latorre, J. Rojo, and M. Ubiali (NNPDF), Nucl. Phys. B **855**, 153 (2012), arXiv:1107.2652 [hep-ph].
- [29] J. Pumplin, D. R. Stump, J. Huston, H. L. Lai, P. M. Nadolsky, and W. K. Tung, JHEP **07**, 012 (2002), arXiv:hep-ph/0201195.
- [30] S. Dulat, T.-J. Hou, J. Gao, M. Guzzi, J. Huston, P. Nadolsky, J. Pumplin, C. Schmidt, D. Stump, and C. P. Yuan, Phys. Rev. D **93**, 033006 (2016), arXiv:1506.07443 [hep-ph].
- [31] R. Wang and X. Chen, Chin. Phys. C **41**, 053103 (2017), arXiv:1609.01831 [hep-ph].
- [32] R. Wang, C. Han, and X. Chen, (2024), arXiv:2407.16122 [hep-ph].
- [33] P.-L. Yin, Y.-Z. Xu, Z.-F. Cui, C. D. Roberts, and J. Rodríguez-Quintero, Chin. Phys. Lett. **40**, 091201 (2023), arXiv:2306.03274 [hep-ph].
- [34] R. Wang and X. Chen, Phys. Rev. D **91**, 054026 (2015), arXiv:1410.3598 [hep-ph].
- [35] J. C. Collins and D. E. Soper, Ann. Rev. Nucl. Part. Sci. **37**, 383 (1987).
- [36] J. C. Collins, D. E. Soper, and G. F. Sterman, Adv. Ser. Direct. High Energy Phys. **5**, 1 (1989), arXiv:hep-ph/0409313.
- [37] G. F. Sterman, in Theoretical Advanced Study Institute in Elementary Particle Physics (TASI) 1995, pp. 327–408, arXiv:hep-ph/9606312. (1995)
- [38] C. S. Armstrong, R. Ent, C. E. Keppel, S. Liuti, G. Niculescu, and I. Niculescu, Phys. Rev. D **63**, 094008 (2001), arXiv:hep-ph/0104055.
- [39] K. D. Lane, Phys. Rev. D **10**, 2605 (1974).
- [40] H. D. Politzer, Nucl. Phys. B **117**, 397 (1976).
- [41] J. M. Cornwall and J. Papavassiliou, Phys. Rev. D **40**, 3474 (1989).
- [42] Y. Nambu and G. Jona-Lasinio, Phys. Rev. **122**, 345 (1961).
- [43] G. Krein, C. D. Roberts, and A. G. Williams, Int. J. Mod. Phys. A **7**, 5607 (1992).
- [44] L. Chang, C. D. Roberts, and D. J. Wilson, PoS **QCDS-TNT-II2011**, 039 (2011), arXiv:1201.3918 [nucl-th].
- [45] C. D. Roberts, Prog. Part. Nucl. Phys. **61**, 50 (2008), arXiv:0712.0633 [nucl-th].
- [46] H. J. Munczek, Phys. Rev. D **52**, 4736 (1995), arXiv:hep-th/9411239.
- [47] D. Binosi, C. Mezrag, J. Papavassiliou, C. D. Roberts, and J. Rodríguez-Quintero, Phys. Rev. D **96**, 054026 (2017), arXiv:1612.04835 [nucl-th].
- [48] Z.-F. Cui, J.-L. Zhang, D. Binosi, F. de Soto, C. Mezrag, J. Papavassiliou, C. D. Roberts, J. Rodríguez-Quintero, J. Segovia, and S. Zafeiropoulos, Chin. Phys. C **44**, 083102 (2020), arXiv:1912.08232 [hep-ph].
- [49] Y. Yu, P. Cheng, H.-Y. Xing, F. Gao, and C. D. Roberts, Eur. Phys. J. C **84**, 739 (2024), arXiv:2402.06095 [hep-ph].
- [50] Y. Lu, L. Chang, K. Raya, C. D. Roberts, and J. Rodríguez-Quintero, Phys. Lett. B **830**, 137130 (2022), arXiv:2203.00753 [hep-ph].
- [51] L. Chang, C. Mezrag, H. Moutarde, C. D. Roberts, J. Rodríguez-Quintero, and P. C. Tandy, Phys. Lett. B **737**, 23 (2014), arXiv:1406.5450 [nucl-th].
- [52] M. Ding, K. Raya, D. Binosi, L. Chang, C. D. Roberts, and S. M. Schmidt, Phys. Rev. D **101**, 054014 (2020), arXiv:1905.05208 [nucl-th].
- [53] Z.-F. Cui, M. Ding, F. Gao, K. Raya, D. Binosi, L. Chang, C. D. Roberts, J. Rodríguez-Quintero, and S. M. Schmidt, Eur. Phys. J. C **80**, 1064 (2020).
- [54] X. Ji, Phys. Rev. Lett. **110**, 262002 (2013), arXiv:1305.1539 [hep-ph].
- [55] X. Ji, Sci. China Phys. Mech. Astron. **57**, 1407 (2014), arXiv:1404.6680 [hep-ph].
- [56] X. Ji, Y.-S. Liu, Y. Liu, J.-H. Zhang, and Y. Zhao, Rev. Mod. Phys. **93**, 035005 (2021), arXiv:2004.03543 [hep-ph].
- [57] X. Ji, J.-H. Zhang, and Y. Zhao, Phys. Rev. Lett. **120**, 112001 (2018), arXiv:1706.08962 [hep-ph].
- [58] Y.-Q. Ma and J.-W. Qiu, Phys. Rev. D **98**, 074021 (2018), arXiv:1404.6860 [hep-ph].
- [59] Y.-Q. Ma and J.-W. Qiu, Phys. Rev. Lett. **120**, 022003 (2018), arXiv:1709.03018 [hep-ph].
- [60] J. Lan, C. Mondal, S. Jia, X. Zhao, and J. P. Vary, Phys. Rev. D **101**, 034024 (2020), arXiv:1907.01509 [nucl-th].
- [61] C. Mondal, S. Xu, J. Lan, X. Zhao, Y. Li, D. Chakrabarti, and J. P. Vary, Phys. Rev. D **102**, 016008 (2020), arXiv:1911.10913 [hep-ph].
- [62] R. J. Holt and C. D. Roberts, Rev. Mod. Phys. **82**, 2991 (2010), arXiv:1002.4666 [nucl-th].
- [63] H. Mineo, W. Bentz, N. Ishii, A. W. Thomas, and K. Yazaki, Nucl. Phys. A **735**, 482 (2004), arXiv:nucl-th/0312097.
- [64] A. C. Aguilar, F. De Soto, M. N. Ferreira, J. Papavassiliou, PoS **QCDS-TNT-II2011**, 040 (2020), arXiv:2004.01595 [hep-ph].
- [65] F. M. Steffens and A. W. Thomas, Prog. Theor. Phys. Suppl. **120**, 145 (1995), arXiv:hep-ph/9509244.
- [66] A. Radyushkin, Annalen Phys. **13**, 718 (2004), arXiv:hep-ph/0410153.
- [67] A. C. Aguilar, F. De Soto, M. N. Ferreira, J. Papavassiliou, PoS **QCDS-TNT-II2011**, 040 (2020), arXiv:2004.01595 [hep-ph].

- iou, J. Rodríguez-Quintero, and S. Zafeiropoulos, Eur. Phys. J. C **80**, 154 (2020), arXiv:1912.12086 [hep-ph].
- [68] A. Bender, C. D. Roberts, and L. Von Smekal, Phys. Lett. B **380**, 7 (1996), arXiv:nucl-th/9602012.
- [69] Y. L. Dokshitzer, Sov. Phys. JETP **46**, 641 (1977).
- [70] V. N. Gribov and L. N. Lipatov, Sov. J. Nucl. Phys. **15**, 438 (1972).
- [71] G. Altarelli and G. Parisi, Nucl. Phys. B **126**, 298 (1977).
- [72] L. V. Gribov, E. M. Levin, and M. G. Ryskin, Phys. Rept. **100**, 1 (1983).
- [73] A. H. Mueller and J.-w. Qiu, Nucl. Phys. B **268**, 427 (1986).
- [74] W. Zhu, Nucl. Phys. B **551**, 245 (1999), arXiv:hep-ph/9809391.
- [75] O. Nachtmann, Nucl. Phys. B **63**, 237 (1973).
- [76] I. Schienbein et al., J. Phys. G **35**, 053101 (2008), arXiv:0709.1775 [hep-ph].